

Inertial effects in discrete sampling information engines

Aubin Archambault, Caroline Crauste-Thibierge, Sergio Ciliberto, Ludovic Bellon
Univ Lyon, ENS de Lyon, CNRS, Laboratoire de Physique, F-69342 Lyon, France

We describe an experiment on an underdamped mechanical oscillator used as an information engine. The system is equivalent to an inertial Brownian particle confined in a harmonic potential whose center is controlled by a feedback protocol which measures the particle position at a specific sampling frequency $1/\tau$. Several feedback protocols are applied and the power generated by the engine is measured as a function of the oscillator parameters and the sampling frequency. The optimal parameters are then determined. The results are compared to the theoretical predictions and numerical simulations on overdamped systems. We highlight the specific effects of inertia, which can be used to increase the amount of power extracted by the engine. In the regime of large τ , we show that the produced work has a tight bound determined by information theories.

1 Introduction

The thermodynamics of feedback controlled systems is a widely studied subject not only for its large number of applications but also for its fundamental aspects [1], which are particularly interesting in mesoscopic systems where thermal fluctuations cannot be neglected. One of these aspects is the connection between information and thermodynamics that goes back to the famous Maxwell demon [2, 3]. Indeed a mesoscopic machine may produce work from its thermal fluctuations using the information on the system state gathered by the feedback. It has been proved that the produced power \dot{w} is always bounded by some information acquisition rate \dot{I} , i.e.

$$\dot{w} \leq k_B T \dot{I}, \quad (1)$$

where k_B is Boltzmann's constant and T the bath temperature [4, 5, 6, 7, 8, 9]. The first inequality of this form was derived by Sagawa and Ueda for a single feedback loop [4], but subsequently has been extended to include the repeated use of feedback [5, 8], allowing for the application to continuously operating information engines. Often I is the mutual information $I_{x,y}$ between the controlled variable x and the outcome y of the measurement performed by

the feedback on the system. However this definition doesn't take into account the relevance of the feedback to the measurement. If the protocol is poorly chosen, the measured information I can be high, while the work extraction will be low. Ashida et al. [9] proposed another extension of the Jarzynski equality, which considers backward processes. They define an unavailable information I_u that is the part of the measured information that is not used to extract work by the chosen protocol. Their generalisation of the Jarzynski equality is the following:

$$\langle \exp \left(-\frac{w}{k_B T} - I + I_u \right) \rangle = \exp \left(\frac{-\Delta F}{k_B T} \right), \quad (2)$$

where ΔF is the free energy difference between the final and initial states. The definition of I used here is not the mutual information but $I(y) = -\log(P(y))$ where $P(y)$ is the probability of getting the measurement outcome y . Instead $I_u = -\log(P_B(y))$ relies on the probability $P_B(y)$ of getting the outcome y of the measurements in the reverse process and is accessible experimentally only if the backward process can be performed.

The properties of Eqs. 1, 2 have been investigated both theoretically [10, 6, 7, 8, 9] and experimentally in several different systems [11, 12, 13, 14, 15, 16, 17, 18, 19, 20]. From the

experimental side the results concerned overdamped systems where the role of inertia can be neglected. In this letter we investigate experimentally several protocols that allow us to produce work from thermal fluctuations in an underdamped system where inertia plays a role. The results are compared with theoretical and numerical results in overdamped systems and although we find several analogies, there are features that pertain only to underdamped systems.

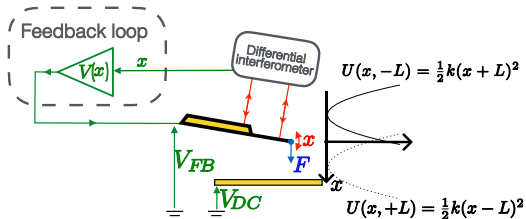


Figure 1: Experimental setup. The deflection of the cantilever x is measured using an interferometer. The deflection is used by the feedback loop to compute a voltage $V_{FB}(x)$ that generates a force on the cantilever, shifting the center of the harmonic potential.

2 Setup

In our experiment a conductive micro-cantilever (Mikromotive Octensis 1000S) acts as an underdamped mechanical oscillator submitted to thermal fluctuations. Fig. 1 sketches our setup, which is similar to the one described in refs. [21, 22]. Specifically the first oscillation mode of the cantilever is used as a underdamped harmonic oscillator characterized by a stiffness $k \simeq 5 \times 10^{-3} \text{ N m}^{-1}$, a resonance frequency $f_0 = 1087 \text{ Hz}$ and an effective mass $m = k/(2\pi f_0)^2$. The quality factor of this oscillator can be tuned by removing the air in the cantilever chamber, from $Q \sim 10$ at atmospheric pressure to $Q \sim 100$ in light vacuum (1 mbar). The tip deflection x follows the dynamics of a 1D underdamped Brownian particle. The standard deviation of x in thermal equilibrium is $\sigma = \sqrt{k_B T/k} \simeq 0.8 \text{ nm}$. In the following, we express all lengths in units of σ and all energies in units of $k_B T$.

The cantilever deflection is measured by an interferometer [23] whose outputs are digitized

and sent to a field programmable gate array device (National Instrument FPGA 7975R) that computes the deflection x [24]. The device can be programmed to output a feedback voltage V_{FB} computed using x and a set of rules implemented by the user. It is linked to a computer that records all the relevant data from the experiment.

The feedback voltage, V_{FB} , output by the FPGA is applied to the cantilever. A DC voltage, $V_{DC} \simeq 90 \text{ V}$ kept constant through all experiments, is applied to a conductive flat surface about $500 \mu\text{m}$ away. This results in a feedback force on the cantilever F_{FB} [25]:

$$F_{FB} \propto (V_{FB} - V_{DC})^2 = (V_{DC}^2 - 2V_{DC}V_{FB} + V_{FB}^2). \quad (3)$$

The term V_{DC}^2 is constant and only shifts the equilibrium position of the oscillator. It is included in changing the reference $x = 0$ to the center of the new harmonic potential. Since the maximum voltage V_{FB} possible for the FPGA is 1 V , $V_{FB}^2 \ll V_{DC}V_{FB}$ and we can further simplify F_{FB} . The resulting expression for the force is $F_{FB} \propto 2V_{DC}V_{FB}$. The DC bias acts as an amplification factor used experimentally to tune the sensitivity of the cantilever to the feedback force.

The delay of the feedback loop is about $1 \mu\text{s}$ which is three order of magnitude smaller than the period of the oscillator $t_0 \simeq 1 \text{ ms}$. Thus the feedback is much faster than the oscillator dynamics [24]. Furthermore the use of the FPGA device allows us to run different experiments with different types of feedback without any modification of the experimental setup configuration.

3 Discrete sampling protocol

Here we focus on a protocol, illustrated in Fig. 2, where the position of the particle x is read by the feedback with a sampling rate τ . Starting from equilibrium with a potential $U(x, -L) = \frac{1}{2}(x+L)^2$ centered in $-L$, at each reading the measured x is compared with a threshold h . If $x < h$, nothing is done and we wait for a time τ before performing a new measurement. If

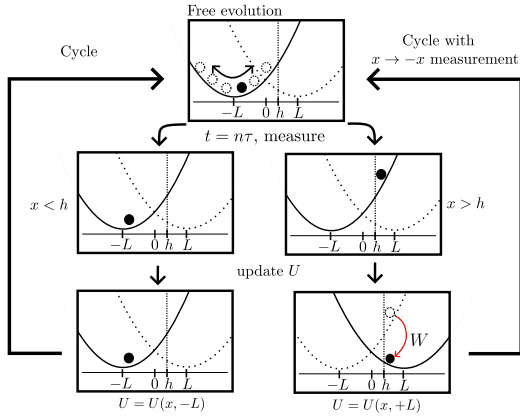


Figure 2: The discrete sampling protocol. Starting with a potential $U(x, -L) = \frac{1}{2}(x + L)^2$ centered in $-L$, every time step τ the position x of the particle is measured. If $x > h$ the potential center is switched from $-L$ to L . In both cases we wait a time τ before performing the next measure.

$x > h$, the potential is instantaneously switched to $U(x, +L) = \frac{1}{2}(x - L)^2$. During this process, the potential energy of the particle is lowered and the internal energy of the particle decreases. Since the potential is switched almost instantaneously, the heat q exchanged by the particle with the bath and the kinetic energy change ΔK are both zero at the switching time. Instead the change in the internal energy of the particle is

$$\Delta U = \frac{1}{2}(x - L)^2 - \frac{1}{2}(x + L)^2 = -2Lx. \quad (4)$$

Since $q = 0$ and $\Delta K = 0$, $\Delta U = -w < 0$ if $x > 0$. By convention, w is defined as the work performed by the particle on the feedback, thus $w > 0$ means that the feedback is extracting work from the particle. The particle is left in the potential centered in L for a time τ . Afterwards a new cycle can be performed symmetrically, switching the potential from $U(x, L)$ to $U(x, -L)$ when $x < -h$.

This protocol is similar to the protocol proposed by T.Sagawa and M.Ueda [4]. The difference between the two protocols is that in our protocol the particle switches back and forth between two potential wells, centered in $\pm L$, whereas the protocol from Sagawa and Ueda uses successive potential wells centered in $-L, L, 3L$, etc.

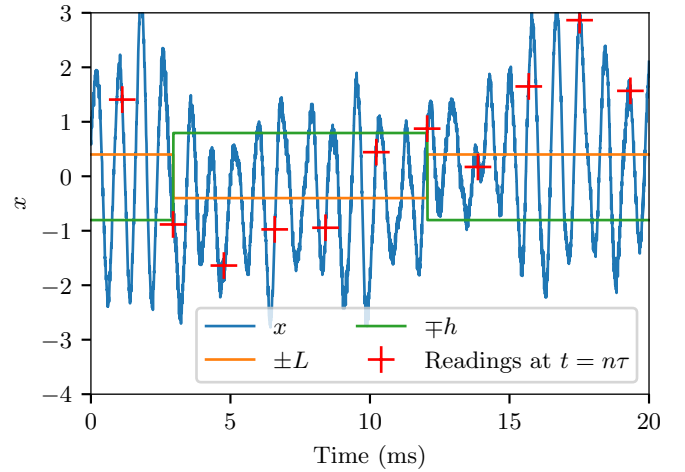


Figure 3: Experimental signals time traces. The blue curve is the measured deflection of the cantilever, x . The orange curve is the position of the center of the potential well and takes values $\pm L$. The green curve takes values $\mp h$ and is the threshold the deflection has to cross for the potential to be switched. Red crosses mark instants when the feedback reads the position of the particle. Since the readings happen only every time τ , the particle can cross the threshold without feedback on the potential if it happens between the readings. Experiments with $\tau \simeq 0.8 t_r = 2 t_0$, $L = 0.4$, $h = 0.8$.

Experimentally, the position of the particle is measured continuously with a sampling frequency of 2 MHz but the feedback is allowed to act only at discrete times with a period τ . Experimental signals are presented in Fig. 3. From the measured trajectory and applied potential, we can compute the work of the particle on the electric field along the trajectory using Stratonovich convention. We can then obtain the statistics of the work performed by the particle each time the potential is switched.

4 Long times limit

We first study the limit $\tau \rightarrow \infty$. This situation corresponds to the case where the particle is back to equilibrium between each reading of the feedback loop. Experimentally, we take $\tau \gtrsim 6 t_r$, where $t_r = Q/(\pi f_0)$ is the relaxation time of the oscillator.

At each reading of x by the feedback loop, we compute the work w extracted by the protocol.

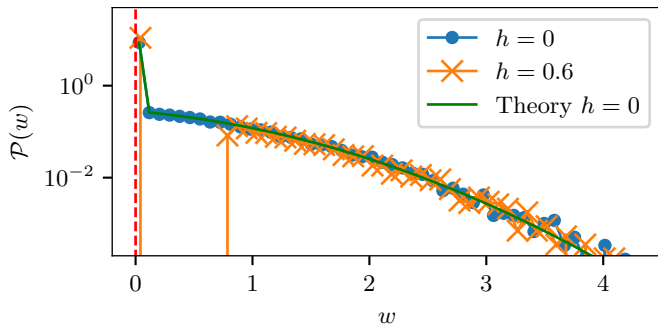


Figure 4: Probability distribution functions of the work performed by the particle at each reading of the feedback loop for $L = 0.6$ with $h = 0$, $h = 0.6$ and $\tau \gtrsim 6 t_r$. The measured pdf is obtained over 10^4 readings of the position. Events are for $w \geq 0$, which corresponds to work extraction. A strong peak in $w = 0$ corresponds to all the readings where $x < h$ and the potential is unchanged, hence $w = 0$.

The probability distribution function (pdf) of w is shown in Fig. 4 for the case $L = 0.6$ and $h = 0$. As expected, all events corresponds to $w \geq 0$ and work is extracted by the feedback. A strong peak is present at $w = 0$ and corresponds to events where the feedback reads a position $x < h$ and does not switch the potential, leading to zero work. There is also a small contribution from events where $x = h = 0$ and the potential is switched with $w = 0$, according to Eq. 4.

The parameters L and h can be chosen to maximize the amount of work and the mean work $\langle w \rangle$ extracted by the feedback at each reading. Fig. 5 shows the extracted work as a function of L at $h = 0$: it presents a maximum in $L = 0.6$. One can also change the position of the threshold h , however the optimal value is $h = 0$. Indeed, if $h < 0$, then we are allowing the system to switch when the particle is in $h < x < 0$ with $w < 0$ according to Eq. 4. In this case, the feedback is providing work to the system to put it in a higher energy state when the potential is switched. If $h > 0$, we are imposing a minimal amount of work $w_0 = 2Lh$ to be extracted each time $x > h$. It means that each time the particle is measured at $0 < x < h$, no work is extracted: $w = 0$. Conversely, if the potential was switched we would have $w > 0$. The feedback is thus losing occasions to extract work. This has been verified experimentally by

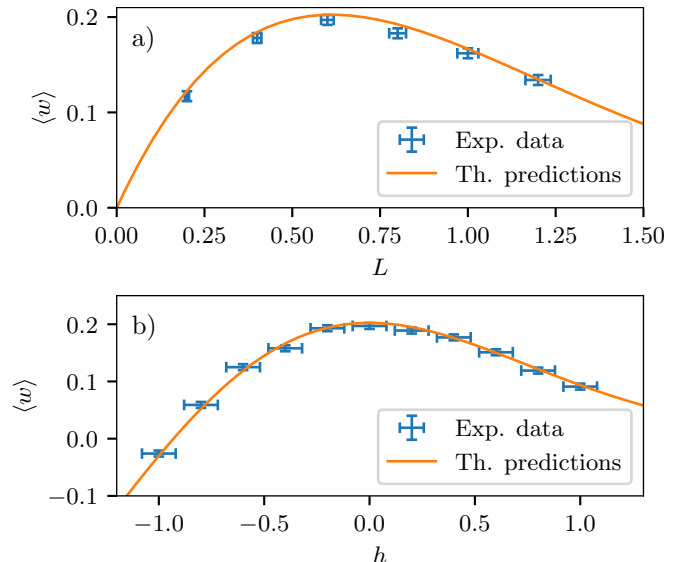


Figure 5: a) Mean work $\langle w \rangle$ as a function of L with $h = 0$ in the limit $\tau \rightarrow \infty$. An optimum appears for $L = 0.6$. b) Mean work $\langle w \rangle$ as a function of the position of the threshold h in the limit $\tau \rightarrow \infty$, for a fixed value of $L = 0.6$.

measuring the extracted power at different values of h and fixed value of $L = 0.6$. The resulting pdf are shown in Fig. 4. The extracted work as a function of h is shown in Fig. 5. As expected the extracted work decreases as soon as $h \neq 0$.

Furthermore, we can easily compare the extracted power to theoretical predictions. Indeed, the distribution of the outcome of the reading is described by the equilibrium distribution in an harmonic potential centered in $-L$, $P_{eq}(x, -L) = \exp(-\frac{1}{2}(x+L)^2)/\sqrt{2\pi}$. From this distribution and using eq. 4, we can deduce the probability distribution of the extracted work:

$$\mathcal{P}(w) = \begin{cases} \frac{1}{2} \left(1 + \operatorname{erf} \left(\frac{L+h}{\sqrt{2}} \right) \right) \delta(w) & \text{if } w = 0, \\ \frac{1}{2L\sqrt{2\pi}} \exp \left(-\frac{1}{2} \left(\frac{w}{2L} + L \right)^2 \right) & \text{if } w > w_0, \\ 0 & \text{if } w < w_0. \end{cases} \quad (5)$$

This distribution is plotted in Fig. 4 for the case $L = 0.6$ and $h = 0$ and shows a perfect agreement to our experimental data. We can also compute the mean extracted work as a function

of L and h :

$$\begin{aligned} \langle w \rangle &= \int_{-\infty}^h 0 \times P_{eq}(x; -L) dx + \int_h^{+\infty} 2Lx \times P_{eq}(x; \\ &= L^2 \left(\operatorname{erf} \left(\frac{L+h}{\sqrt{2}} \right) - 1 \right) + L \sqrt{\frac{2}{\pi}} e^{-\frac{1}{2}(L+h)^2}, \end{aligned} \quad (6)$$

which gives the theoretical curves in Fig. 5.

Since the system has time to relax to equilibrium between each reading by the feedback, there is no memory of the previous reading or of the previous switch in the potential. Therefore it is equivalent to operate back and forth between two potential wells or with successive wells. Furthermore, as all measurements are performed at equilibrium, inertia does not play any role in the limit $\tau \rightarrow \infty$. In this regime our protocol is equivalent to the one of Ref. [4], for which analytical results have been derived by Parks and coworkers [26]. They compute analytically the average work extracted per event for different values of L and h , in the case where $\tau \rightarrow \infty$. They find that the largest work is extracted for $L = 0.6$ and $h = 0$, which corresponds to the result that we obtain experimentally.

5 Intermediate regime

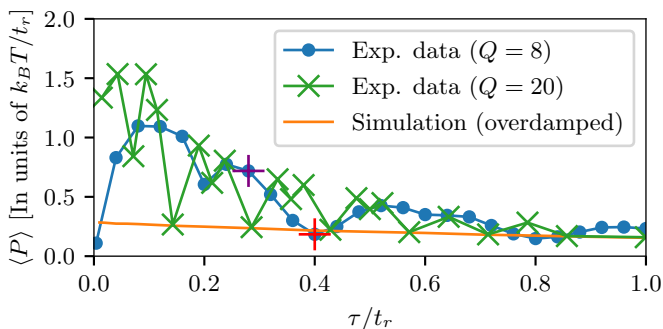


Figure 6: Extracted power as a function of τ in unit of t_r , the relaxation time of the system. In blue, experimental data with $L = 0.6$, $h = 0$ and $Q = 8$ in the underdamped regime. In green, experimental data with $L = 0.6$, $h = 0$ and $Q = 20$. In orange, data from simulations of an overdamped brownian particle.

Operating the engine in a regime of large τ leads to work extraction, but due to the long

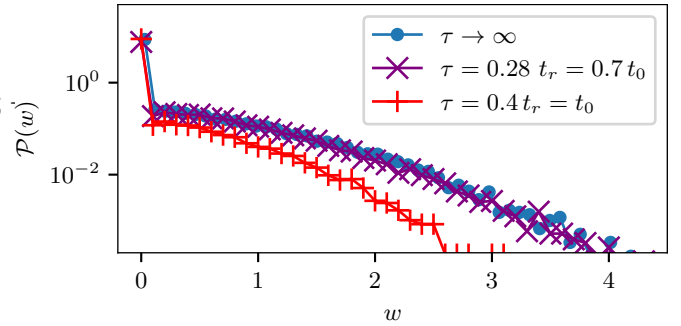


Figure 7: Probability distribution function of extracted work after readings for $L = 0.6$, $h = 0$, $Q = 8$, with $\tau = 0.28 t_r = 0.7 t_0$ (purple) and $\tau = 0.4 t_r = 1 t_0$ (red), compared with the distribution for $\tau \rightarrow \infty$ (blue).

time between cycles, the extracted power $P = \langle w \rangle / \tau$ is very low. A way to increase the power output of the engine is to reduce the time between cycles τ by not letting the system totally relax between cycles. We measure the extracted work while keeping $L = 0.6$ and $h = 0$ fixed but varying the sampling time from $\tau = 0.1 t_0$ to $\tau = 3 t_0$. For comparison, simulations of an overdamped 1D Brownian particle under the same feedback protocol are performed. We simulate the trajectories of overdamped particles for a potential switching between $U(x, -L)$ and $U(x, +L)$, and compute the work extracted for different values of L and h . The simulations are performed using a standard Euler scheme, simulating an overdamped Langevin equation, with viscosity γ , stiffness k , and relaxation time $t_r = \gamma/k$. The simulation starts with a position sampled from equilibrium distribution. Its duration is typically $100 t_r$, the first $5 t_r$ are discarded to reach a steady state, and the time step of the simulation is $dt = 0.004 t_r$. The change of the potential is allowed only every time interval τ which is changed between 0 and t_r . Trajectories from the simulation are then analyzed similarly as the experimental ones. To compare the two results, we use t_r as the unit of time, which is different in the two systems. In the underdamped, inertial, regime $t_r = Q/(\pi f_0)$ while in the overdamped regime $t_r = \gamma/k$. Figure 6 shows the comparison of the power extracted for the two regimes. Using t_r as a unit for times, the curve of the overdamped regime appears as a lower envelope for the curve of

the underdamped regime. The green curve in Fig. 6 shows results from an experiment with higher quality factor ($Q = 20$), obtained by lowering the pressure in the experiment, confirming that t_r is indeed the correct time scale. The extracted power in the underdamped regime is always higher than for the overdamped. This can be understood as in the underdamped regime the system is an oscillator exploring the phase space faster than its overdamped counterpart, thus reaching faster the threshold h .

However, anomalies on the curve appear for the underdamped regime at specific values of τ , where the extracted power drops. To understand these anomalies, we plot on Fig. 7 the pdf of the extracted work for different values of τ : $0.4t_r$ and $0.28t_r$ corresponding respectively to the red and purple crosses on Fig. 6. Two effects can be noticed. First the peak in $w = 0$ is stronger for the anomalous case. This means that more measurements have to be performed before the particle is found on the right side of the threshold. The second effect is that in the anomalous case, the spread of the non-zero part of the pdf is smaller. Since $w = 2Lx$, this means that the particle is found closer to the threshold when the measurement is performed. Both effects contribute to a reduction of the extracted power and can be understood as a synchronisation effect between our measurements and the natural oscillation of the underdamped particle. Indeed, the anomalies of Fig. 6 fall exactly on integer and half-integer values of t_0 , the period of the oscillator, specifically in the example of Fig. 6 at $Q = 8$, $\tau = t_0 \simeq 0.4t_r$.

6 Short times limit

On Fig. 6, we can notice that the power goes to 0 as $\tau \rightarrow 0$. To understand this phenomenon, we did experiments in the regime where $\tau \ll t_r$. This regime, in which x is sampled continuously, can be studied as a first-passage problem of a particle in the potential $U(x, -L)$ [or in $U(x, L)$], whose trajectories start at $-h$ [h], as a result of the previous potential switch, and end at h [$-h$]. Since the comparator reads the position of the system continuously, the excursion of the particle above the threshold is lim-

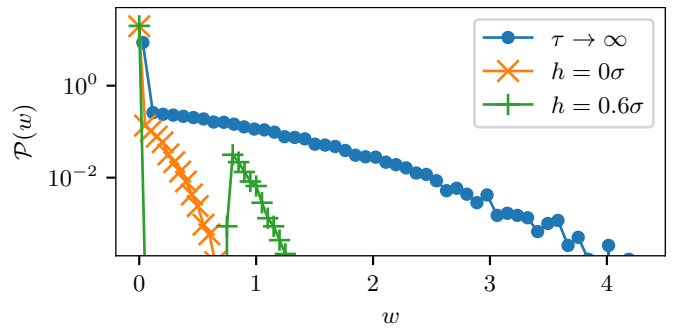


Figure 8: Histograms of work measured at each reading for $\tau = 0.004t_r$, $L = 0.6$ and $h = 0$ (orange curve) and $h = 0.6$ (green curve). Since $\tau \ll t_r$, the potential is switched soon after the particle reaches the threshold, which leads to much narrower distributions compared to the case $\tau \rightarrow \infty$ from figure 4 (reproduced here in blue). The effect of moving the threshold h is that the position of the histogram is switched from around 0 to a non-zero value.

ited and the potential is switched as soon as the particle reaches $x = h$. The work extracted is then $w = 2Lh$ and we can immediately see that if $h = 0$, no work can be extracted as shown by the pdf of the work in Fig. 8. If the threshold is moved to $h > 0$, the work extracted will be non-zero. However, as h is raised, the position of the target threshold is moved away from the initial position, and the time needed for the particle to reach the threshold increases. As a consequence there is an optimal value of h that has to be found.

An experimental map of the power extracted as a function of L and h is displayed in Fig. 9. An optimum for the extracted power is found at $L = 0.6$ and $h = 0.75$, giving an extracted power $P = 1.48k_B T/t_r$. To compare with the overdamped case, we use the same simulation technique as for the intermediate time regime, taking $\tau = dt = 0.004t_r$ for consistency with the experiments. From these simulations, we can compute a map of the extracted power as we do for the experiments. The resulting heatmap is shown in Fig. 9.

A huge difference can be seen between the two regimes. In the overdamped case, the heatmap is dominated by an increase in the extracted power at large L with light dependence on h . Optimal work extraction is achieved for $L =$

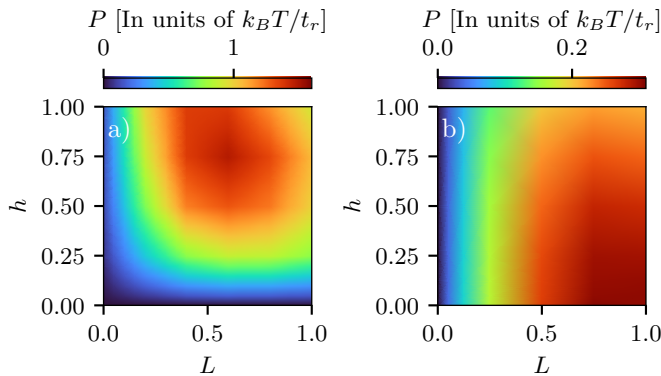


Figure 9: a) Experimental heatmap of the extracted power as a function of L and h for $\tau = 0.004 t_r$ in the underdamped regime. The optimal value is at $L = 0.6$ and $h = 0.75$. b) Computed heatmap of the extracted power as a function of L and h for $\tau = 0.004 t_r$ in the simulated overdamped regime. The optimal value is at $L = 0.75$ and $h = 0$.

0.75 and $h = 0$, giving an extracted power of $P = 0.3 k_B T / t_r$, smaller than the optimum in the underdamped regime. The main difference between the two results is that while in the underdamped regime it is very efficient to work with $h \neq 0$, the overdamped regime is optimal when $h = 0$. This can be understood as in the underdamped regime the dynamic is ballistic, thus the particle crosses 0 with some velocity that will allow the particle to reach a non zero threshold. In the overdamped regime, the viscosity prevents such guesses on the future position of the particle and the optimal is for a threshold in $h = 0$ from the same argument as for $\tau \rightarrow \infty$.

As a conclusion, at small τ the power can be optimized by tuning the values of L and h and in the underdamped case this power becomes very large. It is also interesting to notice that in the overdamped case the largest power is obtained at $L = 0.75$ and $h \rightarrow 0$ which is very different from the values of [26]. It is important to point out that this difference comes from the fact that our system oscillates from $-L$ to L whereas their system translates always in the same direction.

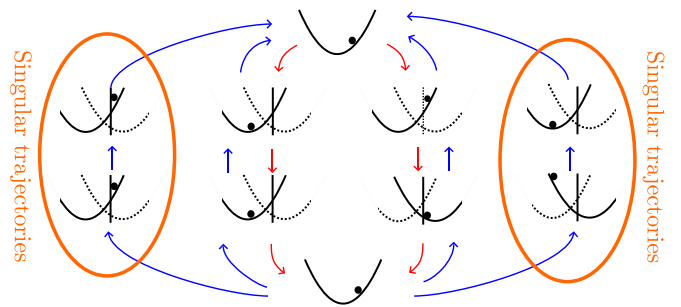


Figure 10: The four kinds of trajectories in our experiments. Two of them are possible in the forward process (red arrow), and two are singular and only possible in the backward process (blue arrow). These singular trajectories corresponds to cases where the particle is above the threshold and the potential is unchanged, or where the particle is below the threshold and the potential is changed.

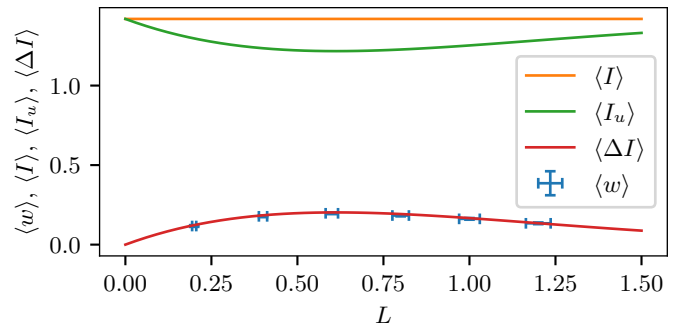


Figure 11: Blue: $\langle w \rangle$ measured experimentally as a function of L in the regime of large τ , with $h = 0$. Orange: Theoretically predicted information I . Green: Theoretical prediction for unavailable information I_u . Red: Comparison with the predicted $\Delta I \equiv I - I_u$.

7 Information

For the case of $\tau \rightarrow \infty$, we can apply the methods from Ashida and coworkers [9]. Our feedback measures exactly the position of the particle x at each reading. The extracted information is then $I(x) = -\log(P_{eq}(x; -L))$. We can notice that $\langle I \rangle$ is independent of the protocol used and is therefore constant throughout our experiments for any value of L or h , as shown on the orange curve of Fig. 11.

For a given measurement, different feedbacks can be applied, resulting in more or less work extraction depending on the smartness of the chosen protocol. In Ref. [9], the notion of unavail-

able information is introduced to give a tighter bound on the extracted work for information engines. Our understanding of this quantity is that it describes the amount of information that is measured from the system but unused by the protocol.

This unused information can be computed by studying the time reversal of the process. In the forward protocol, the outcome m of a measurement at time t_m imposes the protocol λ , which depends on the measurements only at time $t > t_m$. However, in the reverse process, the protocol depends on m at times $t < -t_m$, before the measurement. Due to causality a feedback cannot be performed and the protocol has to be imposed beforehand. This makes some trajectories, that are forbidden in the direct process, possible in the reverse. Such trajectories are called singular trajectories.

For our protocol, there are four kinds of trajectories presented in Fig. 10. The proposed way of computing the unused information I_u in [9] is based on computing the probability of these singular trajectories for a given measurement outcome:

$$I_u = -\log(P(\text{Non-singular trajectories})) \quad (7)$$

In our experiment, this corresponds to an unused information $I_u(x) = -\log(P_{eq}(x; -L))$ for an outcome $x < h$ where the potential is unchanged, and $I_u(x) = -\log(P_{eq}(x; +L))$ for an outcome $x > h$, where the potential is changed.

For measurements where $x < h$, $I(x) = I_u(x)$, and as the potential is unchanged for these trajectories, $w = 0$, which gives $\Delta I = I - I_u = w$. For measurements $x > h$, the potential is changed, which leads to work extraction with $w = 2Lx$. Computing ΔI in this case give $\Delta I = -\log(P_{eq}(x; -L)/P_{eq}(x; +L)) = 2Lx$, which also leads to $\Delta I = w$. Here, I_u catches the dependency of the work extraction on the protocol and depends on the value of L chosen, as illustrated by the green curve on Fig. 11.

We finally have that $w - \Delta I = 0$ for all measurement outcomes and the generalized Jarzynski equality, $\langle e^{w-\Delta I} \rangle = 1$, is satisfied. Fig. 11 shows in blue the experimentally measured $\langle w \rangle$ as a function of L for $\tau = 6t_r$ and $h = 0$ (same data as Fig. 5). We compute and plot in red

the expected value of ΔI as a function of L . We get that ΔI is a tight bound for $\langle w \rangle$ thus the inequality $\langle w \rangle \leq \Delta I$ is saturated. While our protocol might not be optimal and doesn't use all the measured information, no energy is lost by our realization of the protocol and we achieve the maximal work extraction for this given protocol. In this sense we achieve a lossless information engine [17], an engine in which all the used information is converted into extracted work.

8 Conclusion

As a conclusion, we have studied experimentally the behavior of an underdamped harmonic oscillator in presence of thermal noise and a feedback that acts as a demon. Thanks to the demon the harmonic oscillator behaves as an information engine able to produce work from the information gathered by the demon on the state of the system. Several feedback protocols have been applied by tuning the system parameters and the feedback sampling time. We find the optimal choice of the parameters for the underdamped and overdamped oscillators. We show that the relaxation time is the good timescale to compare the two regimes and that the overdamped regime acts as a lower bound for the underdamped regime. Specific synchronisation effects arise when the sampling time is a multiple of the frequency of the underdamped oscillator, making the choice of the sampling time a key parameter when operating underdamped information engine. In the limit of very short sampling times, we highlight strong differences in the optimal parameters for the two regimes. Finally we find that in the limit of very large sampling time the produced work is bounded by the difference between the measured information, which depends on the measurement, and the unused information, which depends on the feedback performed. The same bound is much more difficult to obtain for finite τ and will be the subject of future investigation. While we achieve maximal work extraction for our chosen feedback, it might be possible to increase the efficiency of the engine by using the same measurement with a different feedback, thus lower-

ing the amount of unused information.

Acknowledgments We thank Salambô Dago for the initial programming of the acquisition setup, as well as Alberto Imparato and Christopher Jarzynski for insightful scientific discussions. This work has been supported by project ANR-22-CE42-0022. The data supporting this study will be available in an open public repository upon acceptance of the manuscript.

References

- [1] John Bechhoefer. *Control theory for physicists*. Cambridge University Press, Cambridge, United Kingdom, 2021. OCLC: 1242023038.
- [2] Harvey S. Leff and Andrew F. Rex, editors. *Maxwell's demon: entropy, information, computing*. Adam Hilger, Bristol, 1990.
- [3] Eric Lutz and Sergio Ciliberto. Information: From Maxwell's demon to Landauer's eraser. *Physics Today*, 68(9):30–35, 2015.
- [4] Takahiro Sagawa and Masahito Ueda. Generalized Jarzynski Equality under Nonequilibrium Feedback Control. *Phys. Rev. Lett.*, 104(9):090602, 2010.
- [5] Jordan M. Horowitz and Suriyanarayanan Vaikuntanathan. Nonequilibrium detailed fluctuation theorem for repeated discrete feedback. *Phys. Rev. E*, 82(6):061120, 2010.
- [6] David Abreu and Udo Seifert. Thermodynamics of Genuine Nonequilibrium States under Feedback Control. *Phys. Rev. Lett.*, 108(3):030601, 2012.
- [7] Sourabh Lahiri, Shubhashis Rana, and A M Jayannavar. Fluctuation theorems in the presence of information gain and feedback. *J. Phys. A*, 45(6):065002, 2012.
- [8] Martin Luc Rosinberg and Jordan M. Horowitz. Continuous information flow fluctuations. *Eur. Phys. Lett.*, 116(1):10007, 2016.
- [9] Yuto Ashida, Ken Funo, Yûto Murashita, and Masahito Ueda. General achievable bound of extractable work under feedback control. *Phys. Rev. E*, 90(5):052125, 2014.
- [10] Jordan M. Horowitz and Juan M. R. Parrondo. Thermodynamic reversibility in feedback processes. *Eur. Phys. Lett.*, 95(1):10005, 2011.
- [11] Shoichi Toyabe, Takahiro Sagawa, Masahito Ueda, Eiro Muneyuki, and Masaki Sano. Experimental demonstration of information-to-energy conversion and validation of the generalized Jarzynski equality. *Nat. Phys.*, 6(12):988–992, 2010.
- [12] J. V. Koski, V. F. Maisi, T. Sagawa, and J. P. Pekola. Experimental Observation of the Role of Mutual Information in the Nonequilibrium Dynamics of a Maxwell Demon. *Phys. Rev. Lett.*, 113(3):030601, 2014.
- [13] J. V. Koski, A. Kutvonen, I. M. Khaymovich, T. Ala-Nissila, and J. P. Pekola. On-Chip Maxwell's Demon as an Information-Powered Refrigerator. *Phys. Rev. Lett.*, 115(26):260602, 2015.
- [14] Patrice A. Camati, John P. S. Peterson, Tiago B. Batalhão, Kaonan Micadei, Alexandre M. Souza, Roberto S. Sarthour, Ivan S. Oliveira, and Roberto M. Serra. Experimental Rectification of Entropy Production by Maxwell's Demon in a Quantum System. *Phys. Rev. Lett.*, 117(24):240502, 2016.
- [15] Kensaku Chida, Samarth Desai, Katsuhiko Nishiguchi, and Akira Fujiwara. Power generator driven by Maxwell's demon. *Nat. Comm.*, 8(1):15301, 2017.
- [16] Tamir Admon, Saar Rahav, and Yael Roichman. Experimental Realization of an Information Machine with Tunable Temporal Correlations. *Phys. Rev. Lett.*, 121(18):180601, 2018.

- [17] Govind Paneru, Dong Yun Lee, Tsvi Thusty, and Hyuk Kyu Pak. Lossless Brownian Information Engine. *Phys. Rev. Lett.*, 120(2):020601, 2018.
- [18] M. Ribezzi-Crivellari and F. Ritort. Large work extraction and the Landauer limit in a continuous Maxwell demon. *Nat. Phys.*, 15(7):660–664, 2019.
- [19] Amirhossein Taghvaei, Olga Movilla Miangolarra, Rui Fu, Yongxin Chen, and Tryphon T. Georgiou. On the Relation Between Information and Power in Stochastic Thermodynamic Engines. *IEEE Control Systems Letters*, 6:434–439, 2022.
- [20] Tushar K. Saha, Joseph N. E. Lucero, Jan-nik Ehrich, David A. Sivak, and John Bechhoefer. Bayesian Information Engine that Optimally Exploits Noisy Measurements. *Phys. Rev. Lett.*, 129(13):130601, 2022.
- [21] Salambô Dago, Jorge Pereda, Nicolas Barros, Sergio Ciliberto, and Ludovic Bellon. Information and Thermodynamics: Fast and Precise Approach to Landauer’s Bound in an Underdamped Micromechanical Oscillator. *Phys. Rev. Lett.*, 126(17):170601, 2021.
- [22] Salambô Dago, Jorge Pereda, Sergio Ciliberto, and Ludovic Bellon. Virtual double-well potential for an underdamped oscillator created by a feedback loop. *J. Stat. Mech.: Theory and Experiment*, 2022(5):053209, 2022.
- [23] Pierdomenico Paolino, Felipe A. Aguilar Sandoval, and Ludovic Bellon. Quadrature phase interferometer for high resolution force spectroscopy. *Rev. Sci. Instrum.*, 84(9):095001, 2013.
- [24] Salambô Dago, Nicolas Barros, Jorge Pereda, Sergio Ciliberto, and Ludovic Bellon. Virtual potential created by a feedback loop: taming the feedback demon to explore stochastic thermodynamics of underdamped systems, 2023. arXiv:2311.12687 [cond-mat].
- [25] Hans-Jürgen Butt, Brunero Cappella, and Michael Kappl. Force measurements with the atomic force microscope: Technique, interpretation and applications. *Surf. Sci. Rep.*, 59(1-6):1–152, 2005.
- [26] Jong-Min Park, Jae Sung Lee, and Jae Dong Noh. Optimal tuning of a confined Brownian information engine. *Phys. Rev. E*, 93(3):032146, 2016.